Electronic correlation effects and Coulomb gap in the Si(111)-($\sqrt{3} \times \sqrt{3}$)-Sn surface

A. B. Odobescu,* A. A. Maizlakh, N. I. Fedotov, and S. V. Zaitsev-Zotov
Kotel'nikov IRE RAS, Mokhovaya 11, Building 7, 125009 Moscow, Russia
(Received 15 December 2016; revised manuscript received 31 March 2017; published 23 May 2017)

The electronic transport properties of the Si(111)-($\sqrt{3} \times \sqrt{3}$)-Sn surface formed on the low-doped Si substrates are studied using two-probe conductivity measurements and tunneling spectroscopy. We demonstrate that the ground state corresponds to a Mott-Hubbard insulator with a band gap of $2\Delta \approx 70$ meV, which vanishes quickly upon the temperature increase at $T \sim 30$–40 K. The energy gap at the Fermi level observed in tunneling spectroscopy measurements at higher temperatures could be described in terms of the dynamic Coulomb blockade approximation. The temperature dependence of the surface conductivity above 45 K corresponds to the Efros-Shklovskii hopping conduction law. The obtained localization length of the electron is $\xi \approx 7$ Å.

DOI: 10.1103/PhysRevB.95.195151

I. INTRODUCTION

The two-dimensional (2D) electron gas formed on reconstructed semiconductor surfaces where Coulomb interaction energy is comparable with charge-carrier kinetic energy is a very promising system for the experimental study of the effect of the electron-electron interactions and the electronic transport properties. Of great interest are spin-1/2 antiferromagnetic systems on a 2D triangular lattice, which exhibit many exotic phenomena, such as the formation of spin liquids [1], superconductivity [2], and Mott insulators [3].

An ideal candidate for studying 2D correlated physics on the triangular lattice is an α-phase surface obtained by covering the clean Si(111) surface with the 1/3 monolayer (ML) of Sn adatoms that forms a $\sqrt{3} \times \sqrt{3} - R30^\circ$ reconstruction with ~7-Å interadatom distance. Sn adsorption saturates all the dangling bonds (DBs) of underlying Si surface atoms leaving a single DB per Sn atom with one electron localized on it. For this structure a density functional calculation in the local density approximation (LDA) predicts an undistorted ground metal state [4].

The experimental study of the electronic surface structure by angle-resolved photoemission spectroscopy (ARPES) from 70 to 300 K shows a metallic band structure as expected from the simple electron counting but with a clear indication of 3×3 periodicity [5]. Structural tools, such as scanning tunneling microscopy (STM) and photoelectron diffraction show only $\sqrt{3} \times \sqrt{3}$ periodicity and provide no fingerprints of the 3×3 structure down to 6 K [5,6]. A detailed study [7] with scanning tunneling spectroscopy (STS) and photoelectron spectroscopy at temperatures from 5 to 300 K shows that the electronic structure becomes insulating below 60 K. The discrepancy between the LDA prediction and the experimental results [7] has been resolved in the framework of the local spin-density + Hubbard U approximation [8]. In this approximation the ground state of the Sn/Si(111) surface was found to be a magnetic insulating state.

Recently more precise theories [9–12] have refined the Mott-Hubbard approach to the origin of the insulating state of Sn/Si(111). In Ref. [9] the authors show that the Sn adatom structure reveals the 120° in-plane spiral magnetic configuration pattern with (3×3) symmetry. In Ref. [10] the 120°-Néel noncollinear pattern is obtained on account of spin-orbit coupling. However, in Refs. [11,12] using LDA plus cluster many-body calculations in combination with the ARPES experiment data shows that the insulating ground state has the collinear antiferromagnetic order with a $2\sqrt{3} \times \sqrt{3}$ spin cell. The latest theoretical consideration [13,14] demonstrates that the insulating ground state of Sn/Si(111) can be characterized as a Slater-type insulator via band magnetism due to delocalization of spins over Sn adatoms and Si atoms and the formation of a resonant state through strong orbital hybridization between the Sn $5p_z$ and the Si $3p_z$ orbitals.

The answer to whether the Sn/Si(111) surface is the Slater-type (magnetic order) or the Mott-type (electronic correlations) insulator could be obtained from the transport measurements. A temperature dependence of the conductivity of the Si(111)-($\sqrt{3} \times \sqrt{3}$)-Sn surface shows an insulator behavior in a wide temperature range of 20–300 K with a possible variable-range hopping transport mechanism or activation behavior with a very small activation energy of $2\Delta \approx 10$ meV, which is not uniquely determined [15]. The electronic transport mechanism and the reported activation energy value are not in good agreement with the proposed theories and the STS data [7] where the energy gap is found to be $2\Delta \approx 40$ meV. A similar discrepancy was observed on the metallic Si(111)7×7 surface [16–18] where the origin of the narrow-band gap in the surface states obtained by STS is explained as a result of the Coulomb blockade effect [19]. The Coulomb gap arises when STS is performed on low-conductive surfaces with the sheet conductivity less than the minimum metallic conductivity $1/R_h = e^2/h = 39\ \mu$S [20]. The narrow band gap at the local density of states (LDOS) observed on the Sn/Si(111) surface could also be a result of the Coulomb blockade similar to the Si(111)7×7 scenario.

Here we report the results of a detailed study of the Si(111)-($\sqrt{3} \times \sqrt{3}$)-Sn surface using STS and conductivity measurements. We show that both the temperature dependence of the LDOS measured by STS and the surface conductivity indeed indicate an insulatorlike surface ground state with the surface band gap of $2\Delta \approx 70$ meV. At $T \sim 30$–40 K the insulator state vanishes due to thermal fluctuation, and the surface turns into a bad metal.

*arty@cplire.ru

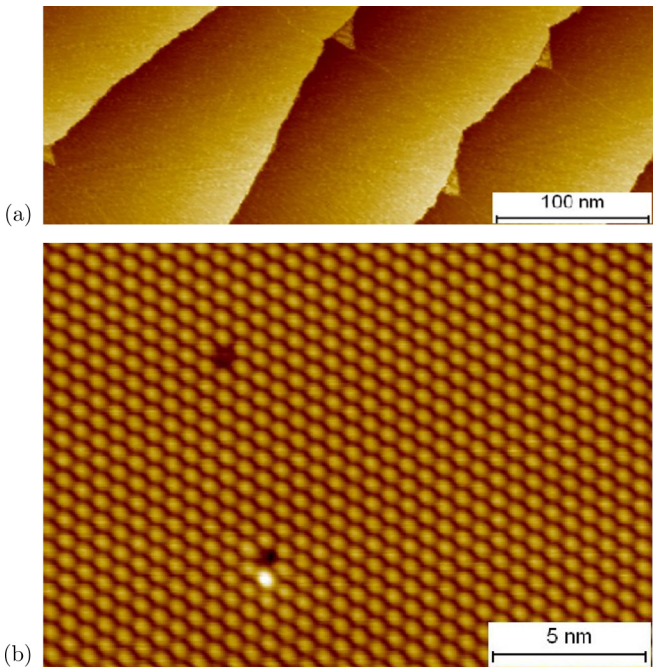

FIG. 1. STM images of the Si(111)-($\sqrt{3} \times \sqrt{3}$)-Sn surface with different exposition times during Sn evaporation: (a) The extra Sn-deposited adatoms form triangular islands of the ($\sqrt{7} \times \sqrt{3}$)-Sn phase near terrace edges $T = 78$ K; (b) the clean Si(111)-($\sqrt{3} \times \sqrt{3}$)-Sn structure with an average defect concentration less than 2%, and the image is obtained at $T = 5$ K under external illumination of the surface. Substrate Si n type, $\rho = 1$ Ωcm, $V_T = -2$ V, $I_T = 50$ pA.

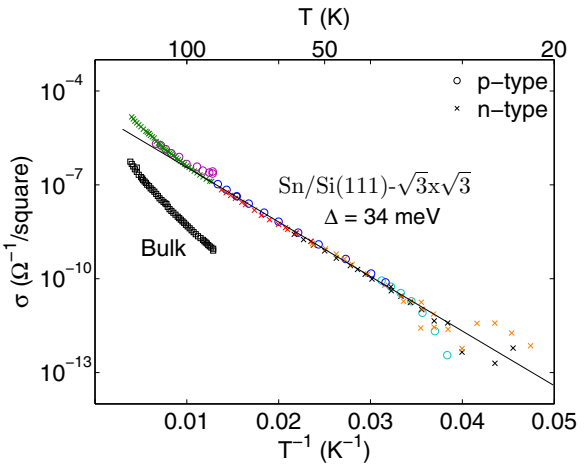

FIG. 2. Temperature variation of the surface conductivity of the clean Si(111)-($\sqrt{3} \times \sqrt{3}$)-Sn structure obtained using two-point microprobes for n-type (crosses) and p-type (circles) Si substrates with $\rho = 1\ \Omega$ cm. Different colored markers correspond to the individual measurements performed with various two-point microprobes on each time-freshly prepared surfaces. The black squares showing the results of the two-point measurements of the Si(111)-($\sqrt{3} \times \sqrt{3}$)-Sn surface degraded in the vacuum chamber for 7 days indicate the upper boundary for the contribution of the bulk and subsurface layer into the measured conductivity.

II. EXPERIMENT

The tunneling spectroscopy measurements were performed in a commercial UHV LT STM Omicron. We used low-doped n- and p-type Si crystals with $\rho = 1\ \Omega$ cm as the substrate in order to eliminate the contribution of the bulk conductivity at low temperatures in electron transport measurements and the effect of charge-carrier concentration change due to the band bending near the surface [21]. Such crystals are insulating in the low-temperature region and cannot be studied by the STM technique. Therefore, for the STM and STS study we used the external illumination to produce necessary bulk conduction at low temperatures (see the details below).

The Si(111)-(7 × 7) clean surface was prepared by direct current heating up to 1250 °C for 30 s and computer-controlled cooling. Then the 1/3 ML of Sn was deposited at room temperature on the surface and annealed at 600 °C for 5 min to create the Si(111)-($\sqrt{3} \times \sqrt{3}$)-Sn reconstructions. To eliminate the ($\sqrt{7} \times \sqrt{3}$)-Sn phase growth near the step edges [Fig. 1(a)] the necessary quantity of deposited Sn was fitted by reducing the evaporation time until the ($\sqrt{7} \times \sqrt{3}$)-Sn phase disappears completely. All STM and STS measurements were performed with platinum STM tips, preliminarily tested on Au foil to verify spectroscopy and microscopy capabilities. The I-V curves were collected at a fixed temperature over the adatom of the Si(111)-($\sqrt{3} \times \sqrt{3}$)-Sn unit cell far away from defects and averaged over a series of measurements consisting of tens of individual cycles. The data collected over the individual defects are the same. The dI/dV were measured with a lock-in technique with a sinusoidal modulation of the sample bias voltage with amplitudes of 30–50 mV at a frequency of $f = 778$ Hz and verified by comparison with calculated numerically dI/dV from averaged I-V curves.

The temperature-dependent transport measurements were performed with a two-probe technique using the Omicron LT SPM with a modified standard tip holder, equipped with two ⊘30-μm platinum wire contacts. The distance between point contacts was $l \approx 400\ \mu$m. The I-V curves were measured using a picoammeter Keithley 6487 with an integrated voltage source at fixed sample temperatures controlled by a LakeShore 325 temperature controller. In approximation of low conductive bulk the total conductivity accounts for only 2D geometrical spreading resistance of the surface: $\sigma_{2p} = \frac{I}{\pi V} \ln(\frac{l}{d})$, where d is the contact spot size. We take $\ln(l/d) \approx 4.4$, which corresponds to $d = 1 - 30\ \mu$m within 30% accuracy. The contribution of the bulk conductivity into the measured data for used low-doped samples was found to be negligibly small at low temperatures: A control measurement obtained for the surface degraded at vacuum condition for 7 days is shown in Fig. 2. The conductivity of the bulk plus contribution through the degraded surface is more than two orders of magnitude smaller than the clean surface conductivity below $T = 100$ K. This gives the bulk contribution to be below 1%. The choice of the two-probe technique let us extend the measurements over seven orders of surface conduction variation into a region of very low conductivity not available with the usual four-probe technique.

To perform spectroscopy measurements at helium temperatures we used external illumination from a typical light-emitting diode source with light intensity up to 10^{-4} W cm^2 at the sample position. This provides necessary conduction of the

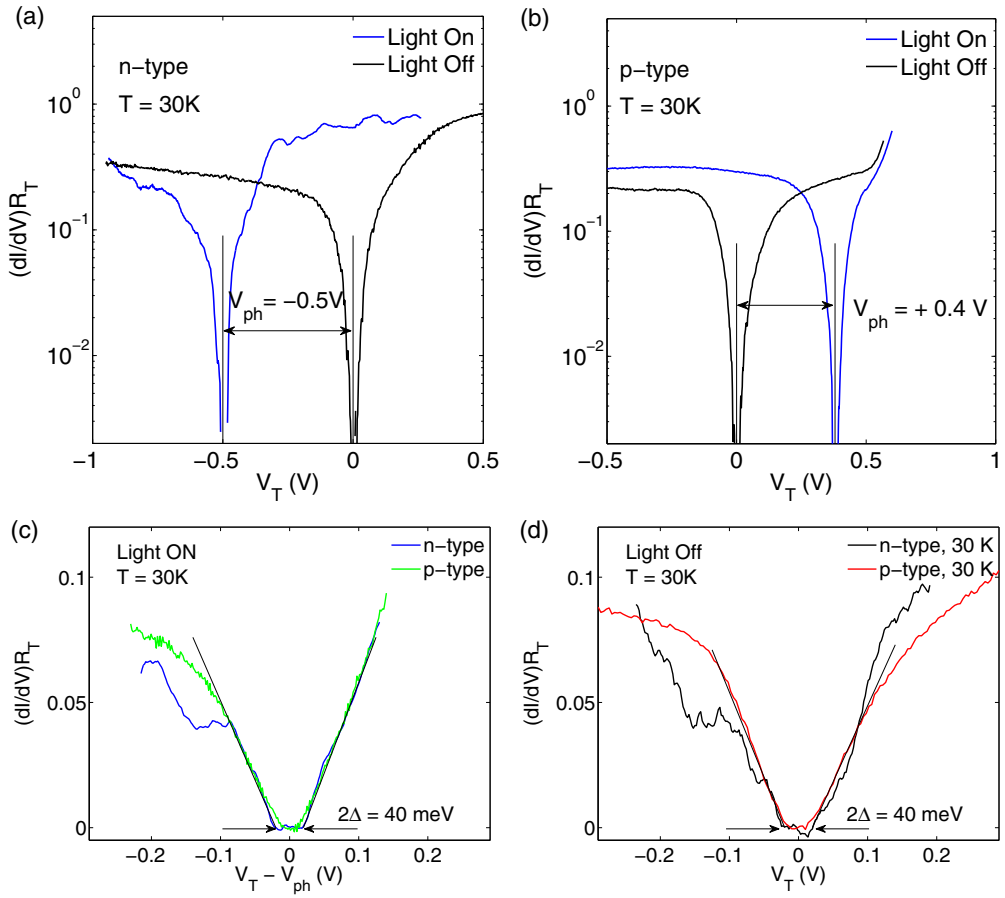

FIG. 3. (a) and (b) The STS spectra $(dI/dV)R_T$ of the Si(111)-($\sqrt{3}\times\sqrt{3}$)-Sn surface obtained at $T = 30$ K on illuminated (blue lines) n- and p-type samples and the same point with no external illumination (black lines). (c) and (d) STS spectra in the vicinity of the energy gap developed at the Fermi level on the Si(111)-($\sqrt{3}\times\sqrt{3}$)-Sn surface for n- and p-type samples measured when illumination is on and off. Set point parameters are $V_T = -2$ V, $I_T = 50$ pA for the n type and $V_T = 1.8$ V, $I_T = 50$ pA for the p type.

bulk required for the STS and STM study and removes bands bending near the surface and restores initial charge-carrier concentration in the surface bands [22,23]. Illumination-induced shift of the surface bands energy positions by photovoltage (Fig. 3) was taken into account.

III. RESULTS

Figure 2 shows the temperature dependence of the surface conductivity of the Si(111)-($\sqrt{3}\times\sqrt{3}$)-Sn surface measured on n- and p-type samples with various two-point probes in the temperature range of 25–260 K. At $20 < T \lesssim 80$ K the conductivity corresponds to activation law $\sigma \propto \exp(-\frac{\Delta}{kT})$ with the activation energy of $\Delta = 34 \pm 1$ meV, which is the same for both n- and p-type samples. At lower temperatures ($T < 25$ K) the conductivity of the surface drops below the measurement limit of the used picoammeter. The 25 K also was the limit for the STM measurements without using external illumination of our samples.

Figure 3 shows the STS data sets measured at $T = 30$ K with and without external illumination. The energy gap at zero voltage is seen clearly on both data sets collected in the dark. When the samples are illuminated, the energy gap is shifted by the value of surface photovoltage $V_{ph} = -0.5$ and $V_{ph} = 0.4$ V fothe n and p samples, respectively. The values of the photoshifts indicate that the Shottky barrier near the surface almost completely disappears. We observed no noticeable deviation in the shape and value of the energy gap measured with and without external illumination [Figs. 3(c) and 3(d)]. The value of the gap at $T = 30$ K is $2\Delta \approx 40$ meV similar with that reported in Ref. [7] obtained on heavily doped Si samples at $T = 5$ K.

At lower temperatures it was impossible to detect any surface states inside the bulk gap. The typical characteristic dI/dV spectra of the bulk are plotted in Fig. 4(c). The explanation for this is very low surface conductivity at helium temperatures and possible high resistance at contact sample-holder $R_{\text{bulk-hold}}$, comparable with tunneling resistance R_{tun}. In this case the bias voltage V_T is distributed partially between the vacuum tunneling junction and the (bulk Si)-(metallic sample-holder) junction [Fig. 4(a)]. By altering the distance between the tip and the surface the $V_{\text{bulk-hold}}$ part could be extracted and used for correction of the dI/dV data. The method is described in detail in Ref. [17]. Namely, we measured $I(V)$ spectra at distances shifted from the set point at $I_T = 50$ pA, $V_T = 2$ V, $R_T = 4\times10^{10}$ Ω at $\Delta Z = -1$, and $\Delta Z = +1$ Å [(Fig. 4(b)]. Then $I(V_{\text{tip-surface}})$ is calculated by the subtraction of $I(V_{\text{bulk-hold}})$ from $I(V_T)$ measured at

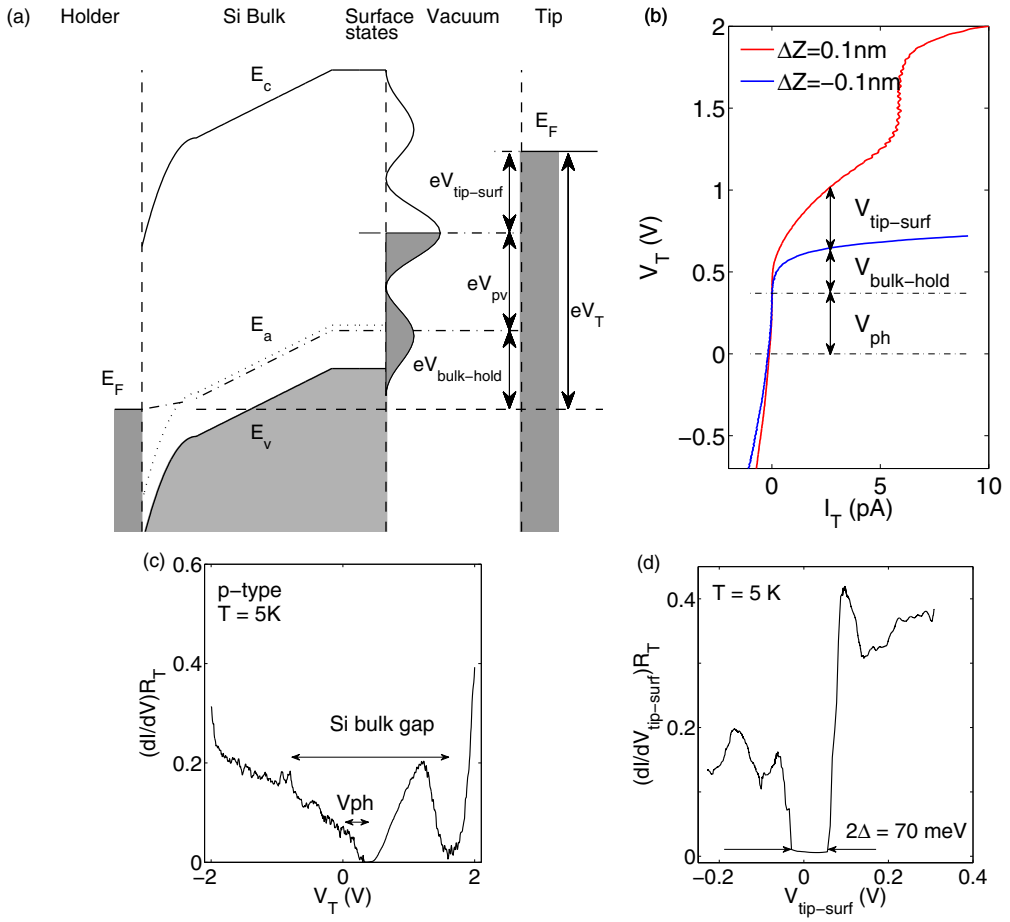

FIG. 4. (a) A schematic energy diagram of the tip-surface-sample-holder bias voltage distribution of the illuminated sample when the resistance of the bulk-holder part is comparable with the vacuum junction resistance; (c) normalized dI/dV data taken at the set point $\Delta Z = 0$ Å, $I_T = 50$ pA, $V_T = 2$ V; (b) the I/V data of the same point taken at different tip-sample distances shifted from the set point at ΔZ. (d) Corrected normalized conductance $(dI/dV_{\text{tip-surface}})R_T$ of the Sn/Si(111) surface at $T = 5$ K.

higher tunneling distances [Fig. 4(d)]. Then the energy gap value varying from 70 to 100 meV for both n- and p-type substrates was obtained from numerically calculated $(dI/dV_{tip\text{-}surface})R_T$ spectra.

Another method is to decrease the bulk-holder resistance by preliminary evaporation of Ta contact areas on the studied sample surface so that the holder plates mount to these Ta areas. In this case the $I(V)$ spectra was found not to be affected by the tip-surface distance, and the surface states could be distinguished in the bulk gap region. The resulting normalized dI/dV spectra are shown in Fig. 5. The energy gap values obtained by this method are $2\Delta \approx 70$ meV for the p-type sample and $2\Delta \approx 90$ meV for the n-type sample.

IV. DISCUSSION

The measured value of the energy gap in the LDOS for the Si(111)-$\sqrt{3} \times \sqrt{3}$-Sn surface at helium temperature is $2\Delta \approx 70$–90 meV and agrees well with the activation energy obtained in the transport measurements of $\Delta = 34 \pm 1$ meV. So the ground state corresponds to an insulator-type state. According to Ref. [8] the insulator state occurs due to spin ordering, which should disappear with a temperature increase due to thermal fluctuations. The intersite antiferromagnetic exchange-coupling energy is $J \sim 3$ meV, so vanishing of this state at $T \gtrsim J \approx 40$ K is expected. The next phase for the

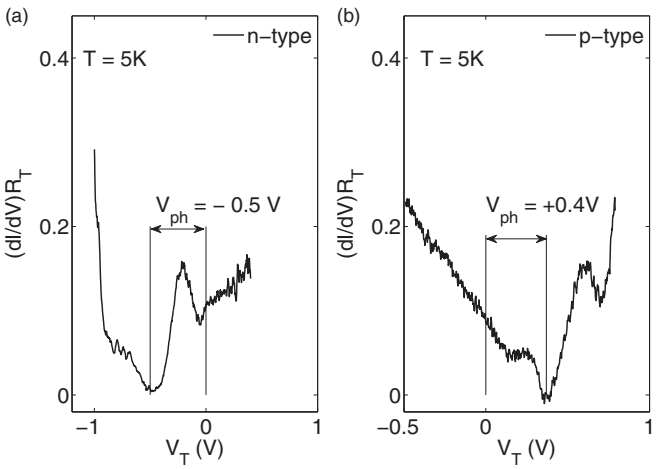

FIG. 5. The normalized $(dI/dV)R_T$ data of the illuminated Si(111)-($\sqrt{3} \times \sqrt{3}$)-Sn surface with preliminary deposited Ta contact areas $T = 5$ K. (a) n-type, (b) p-type Si substrates with $\rho = 1\ \Omega$ cm. Set points: $V_T = -2$ V, $I_T = 50$ pA for the n type; $V_T = 1.8$ V, $I_T = 50$ pA for the p type.

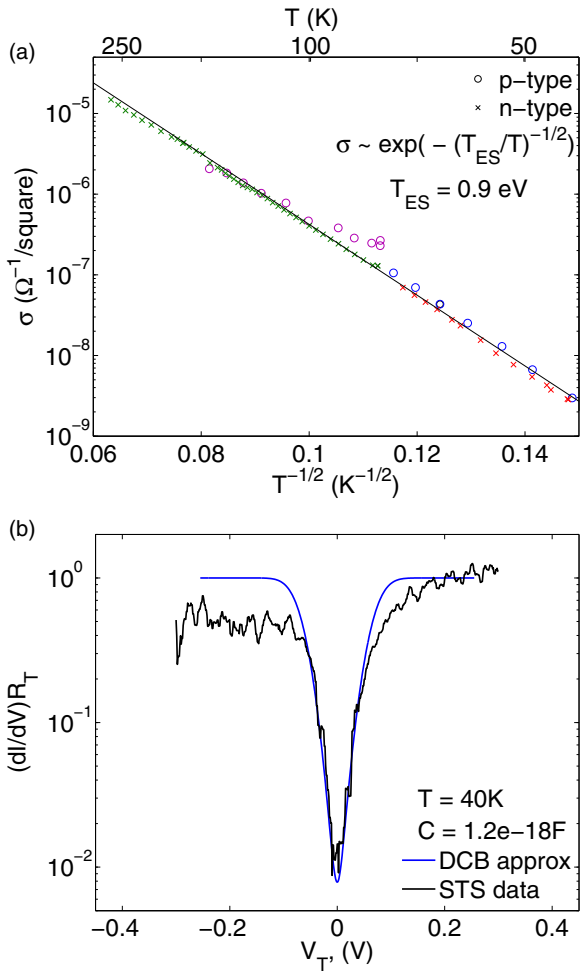

FIG. 6. (a) The temperature variation of the Si(111)-($\sqrt{3} \times \sqrt{3}$)-Sn surface conductivity presented with $\ln\sigma(T^{-1/2})$ coordinates. The data correspond to the Efros-Sklovskii hopping conduction; (b) the deep valley at the surface Fermi level in normalized $(dI/dV)R_T$ spectra of the Si(111)-($\sqrt{3} \times \sqrt{3}$)-Sn surface at $T =$ 40 K (the black line) fitted within the dynamic Coulomb approximation with $C_{\text{surf}} = 1.2 \times 10^{-18}$ °F, $R_{\text{surf}} = 4 \times 10^4 R_h$, $T =$ 40 K. $V_T = -1.8$ V, $I_T = 50$ pA sample n-type Si.

Si(111)-($\sqrt{3} \times \sqrt{3}$)-Sn surface is a pseudogap metal. The conductivity is expected to be the variable-range hopping conduction affected by strong Coulomb interaction if the electrons are localized on Sn dangling bonds. Indeed, our data indicate the Efros-Shklovskii temperature-dependent conductivity $\sigma \sim \exp[-(T_{ES}/T)^{1/2}]$ above $T \gtrsim 45$ K [Fig. 6(a)] is in good agreement with our suggestion. The estimated $T_{ES} \approx$ 0.9 eV corresponds to the localization length of the charge-carrier $\xi = \frac{2.8e^2}{\kappa T_{ES}} = 7.3 \pm 0.3$ Å [24], where $\kappa = (11.8 + 1)/2$ is the dielectric constant of the Si bulk plus vacuum. The localization length precisely matches the distance between Sn adatoms, which is very similar to what was observed on the Si(111)-(7 × 7) surface [19]. The deep valley at zero bias observed in tunneling LDOS at higher temperatures ($T \gtrsim 40$ K) is not connected anymore to the band gap of the insulator ground state but could be described in terms of the dynamic Coulomb blockade approximation as a sequential single-electron tunneling into a low conductive surface with sheet conduction $\sigma \ll e^2/h$. In this approximation the surface is presented as the resistance R_{surf} and the capacitance C_{surf} (for more details, see Refs. [20,25]). The STS data at $T = 40$ K fitted within the dynamic Coulomb approximation using the only one fitting parameter C_{surf} is presented in Fig. 6(b). For higher temperatures the data also fit well within $C_{\text{surf}} = 1.1 \times 10^{-18}$–$1.2 \times 10^{-18}$ °F. The relevant localization length a of the tunneled electron could be estimated as $a \sim C/8\pi\kappa\varepsilon_0 \approx 8.1 \pm 0.8$ Å [26]. The value agrees perfectly with the localization length obtained from the transport measurements.

V. CONCLUSION

In conclusion, through the analysis of transport conductance measurements and tunneling spectroscopy data of the Si(111)-($\sqrt{3} \times \sqrt{3}$)-Sn surface formed on low-doped Si samples, we found that the ground state of this surface is insulating with the surface band gap of $2\Delta \approx 70$ meV. With increasing the temperature the insulator state vanishes due to thermal fluctuation and the surface turns into a bad metal with a Coulomb gap at the Fermi level. The temperature dependence of the surface conductance corresponds to the Efros-Shklovskii hopping conduction at $T \gtrsim 40$ K, and the deep valley in the STS data is described in terms of the dynamic Coulomb approximation. The obtained localization length in both methods agrees perfectly with the interatomic Sn adatoms' distance. Our data indicate the electronic correlations play a crucial role in electronic properties of the Sn/Si(111) surface, so we lean towards the view that the origin of the insulator ground state is more consistent with the Mott-type insulator state with possible localized magnetism driven by strong electron correlations within the Sn overlayer [12] rather than the Slater-type insulator state via an itinerant magnetism [14].

ACKNOWLEDGMENT

The work was supported by the Russian Foundation for Basic Research under Contract No. 16-32-60156.

[1] L. Balents, Nature (London) **464**, 199 (2010).
[2] T. Zhang, P. Cheng, W.-J. Li, Y.-J. Sun, G. Wang, X.-G. Zhu, K. He, L. Wang, X. Ma, X. Chen, Y. Wang, Y. Liu, H.-Q. Lin, J.-F. Jia, and Q.-K. Xue, Nat. Phys. **6**, 104 (2010).
[3] A. Tejeda, Y. Fagot-Révurat, R. Cortés, D. Malterre, E. G. Michel, and A. Mascaraque, Phys. Status Solidi A **209**, 614 (2012)
[4] G. Profeta, A. Continenza, L. Ottaviano, W. Mannstadt, and A. J. Freeman, Phys. Rev. B **62**, 1556 (2000).

[5] R. I. G. Uhrberg, H. M. Zhang, T. Balasubramanian, S. T. Jemander, N. Lin, and G. V. Hansson, Phys. Rev. B **62**, 8082 (2000).
[6] H. Morikawa, I. Matsuda, and S. Hasegawa, Phys. Rev. B **65**, 201308 (2002).
[7] S. Modesti, L. Petaccia, G. Ceballos, I. Vobornik, G. Panaccione, G. Rossi, L. Ottaviano, R. Larciprete, S. Lizzit, and A. Goldoni, Phys. Rev. Lett. **98**, 126401 (2007).
[8] G. Profeta and E. Tosatti, Phys. Rev. Lett. **98**, 086401 (2007).
[9] P. Hansmann, T. Ayral, L. Vaugier, P. Werner, and S. Biermann, Phys. Rev. Lett. **110**, 166401 (2013).
[10] D. I. Badrtdinov, S. A. Nikolaev, M. I. Katsnelson, and V. V. Mazurenko, Phys. Rev. B **94**, 224418 (2016).
[11] G. Li, M. Laubach, A. Fleszar, and W. Hanke, Phys. Rev. B **83**, 041104 (2011).
[12] G. Li, P. Höpfner, J. Schäfer, C. Blumenstein, S. Meyer, A. Bostwick, E. Rotenberg, R. Claessen, and W. Hanke, Nat. Commun. **4**, 1620 (2013).
[13] J.-H. Lee, H.-J. Kim, and J.-H. Cho, Phys. Rev. Lett. **111**, 106403 (2013).
[14] J.-H. Lee, X.-Y. Ren, Y. Jia, and J.-H. Cho, Phys. Rev. B **90**, 125439 (2014).
[15] T. Hirahara, T. Komorida, Y. Gu, F. Nakamura, H. Idzuchi, H. Morikawa, and S. Hasegawa, Phys. Rev. B **80**, 235419 (2009).
[16] R. Losio, K. N. Altmann, and F. J. Himpsel, Phys. Rev. B **61**, 10845 (2000).
[17] S. Modesti, H. Gutzmann, J. Wiebe, and R. Wiesendanger, Phys. Rev. B **80**, 125326 (2009).
[18] T. Tanikawa, K. Yoo, I. Matsuda, S. Hasegawa, and Y. Hasegawa, Phys. Rev. B **68**, 113303 (2003).
[19] A. B. Odobescu, A. A. Maizlakh, and S. V. Zaitsev-Zotov, Phys. Rev. B **92**, 165313 (2015).
[20] P. Joyez and D. Esteve, Phys. Rev. B **56**, 1848 (1997).
[21] Current carrier concentration change $\Delta Q = d \times N_a$, where $d = \sqrt{\frac{2\kappa\varepsilon_0 \Delta E}{e^2 N_a}}$ is the depletion depth and N_a is the—dopant concentration in the substrate $\Delta E \approx 0.4$ eV—band bending value. For heavily doped Si with $\rho = 0.001\ \Omega$ cm the carrier concentration change on the $(\sqrt{3} \times \sqrt{3})$-Sn surface is estimated about 10%.
[22] A. B. Odobescu and S. V. Zaitsev-Zotov, J. Phys.: Condens. Matter **24**, 395003 (2012).
[23] S. Grafström, J. Appl. Phys. **91**, 1717 (2002).
[24] B. I. Shklovskii and A. L. Efros, *Electronic Properties of Doped Semiconductors* (Springer-Verlag, Berlin, 1984).
[25] C. Brun, K. H. Müller, I.-P. Hong, F. Patthey, C. Flindt, and W.-D. Schneider, Phys. Rev. Lett. **108**, 126802 (2012).
[26] The capacitance of a tiny disk with characteristic dimension a describes the spreading area of a tunneled electron before the next tunneling event is estimated as $C = 8a\pi\kappa\varepsilon_0$.